energies

Article

DSVM-Based Model-Free Predictive Current Control of an Induction Motor

Md Asif Hussain [1], Ananda Shankar Hati [1,*], Prasun Chakrabarti [2,*], Bui Thanh Hung [3], Vadim Bolshev [4,5] and Vladimir Panchenko [6]

[1] Department of Electrical Engineering, Indian Institute of Technology (Indian School of Mines), Dhanbad 826004, India
[2] Department of Computer Science and Engineering, ITM SLS Baroda University, Vadodara 391510, India
[3] Data Science Department, Faculty of Information Technology, Industrial University of Ho Chi Minh City, Ho Chi Minh City 71409, Vietnam
[4] Laboratory of Intelligent Agricultural Machines and Complexes, Don State Technical University, 344000 Rostov-on-Don, Russia
[5] Federal Scientific Agroengineering Center VIM, 109428 Moscow, Russia
[6] Department of Theoretical and Applied Mechanics, Russian University of Transport, 127994 Moscow, Russia
* Correspondence: anandashati@iitism.ac.in (A.S.H.); drprasun.cse@gmail.com (P.C.)

Abstract: Classical model-free predictive current control (MFPCC) is a robust control technique for a two-level inverter-fed induction-motor drive, with advantages that consist of a simple concept, rapid response, simple implementation, and excellent performance. However, the classic finite-control-set MFPCC still exhibits a significant current ripple. This article presents a method to enhance performance using a combination of model-free predictive current control (MFPCC) and discrete-space vector modulation (DSVM). The MFPCC employs an ultralocal model with an extended-state observer (ESO) that does not consider motor parameters, therefore improving the control system's reliability by eliminating the parameter dependency. The proposed method integrates DSVM, which divides a single sample period into N equal intervals and generates virtual vectors to reduce stator current ripple. It achieves the minimum cost-function value across the entire operating range of the induction-motor (IM) drive by selecting the optimal vector from a limited set of permissible voltage vectors. Using DSVM effectively reduces the total harmonic distortion (THD) without any detrimental effects during transients or steady states. Experimental studies validate the effectiveness and superiority of the suggested technique over the Finite-Control-Set (FCS) MFPCC, which only considers real voltage vectors in its computations.

Keywords: model-free predictive current control (MFPCC); induction motor; current control; robustness; discrete-space vector modulation (DSVM); observers

check for updates

Citation: Hussain, M.A.; Hati, A.S.; Chakrabarti, P.; Hung, B.T.; Bolshev, V.; Panchenko, V. DSVM-Based Model-Free Predictive Current Control of an Induction Motor. *Energies* **2023**, *16*, 5657. https://doi.org/10.3390/en16155657

Academic Editor: Frede Blaabjerg

Received: 28 June 2023
Revised: 24 July 2023
Accepted: 25 July 2023
Published: 27 July 2023

1. Introduction

The industrial sector has embraced induction motors for their flexibility, low maintenance needs, and longevity. As a result, various control strategies for induction motors have been extensively studied in the literature, each offering unique features and characteristics. Model Predictive Control (MPC) has received considerable attention in power converters and induction-motor drives due to its intuitive nature and broad applicability over the past decade. MPC techniques can be classified into two categories within this domain, reflecting their disparate approaches and potential applications, and the distinction between the two is determined by the method used to generate the switching signals that control the operation of the power converters [1,2]. In one implementation, the predictive algorithm is essential for generating reference outputs that function as modulation step inputs. By utilizing the switched nature of power converters, an alternative model predictive control technique eliminates the need for modulation, enabling the selection of a restricted set of output states. Considering the application's specific control objectives and limitations, the optimal condition is determined by evaluating these states thoroughly. This technique is known as finite-control-set model predictive control (FCS-MPC), first described in [3,4]. Finite-control configuration MPC is the only MPC method that considers an inverter's discrete character and provides the optimal solution to the online optimization problem. For motor drives, predictive control can be categorized as either current control or direct torque control, with the performance of both methods being exceptional despite certain limitations [5]. For applications such as ventilation systems, pumping systems, and air compressor systems, predictive current control (PCC) is favorable to direct torque control for variable-speed drives. Moreover, this strategy integrates constraints and nonlinearities, and its digital implementation is simple enough [6].

Due to FCS-MPC being nonlinear, it is impossible to determine the effect of parameter variations using widely recognized analysis techniques relevant to linear systems. Hence, the influence of model–parameter mismatch has been analytically assessed in prior research by analyzing FCS-MPC behavior under various uncertainty states. Applications have been studied, including current prediction and control for three-phase two-level inverters, multi-level voltage–source converters, active front-end converters, and multiphase electric motors. However, MPC significantly depends on the precision of the machine parameters. The operating point and environment may influence the machine's parameters; for instance, meteorological conditions can impact the stator resistance and inductance of the motor. In addition, for example, because the environment of underground mines is too harsh, underground mining equipment such as auxiliary fans, conveyor belts, and other machinery might adversely affect the system's overall effectiveness [7–10].

Numerous control strategies have been published in the literature to address the problem of parameter dependence. For instance, the online parameter identification method, online parameter estimation, and autotuning of a discrete-time model for induction-motor drives are proposed, in addition to multi-objective parameter estimation [11]. However, online parameter identification necessitates enormous mathematical calculations, leading to the system's complexity, and the identification correctness directly impacts the system's control performance [12].

Recently, the model-free control strategy suggested by Fliess and Join received significant interest in intelligent transportation, energy system management, and other fields [13]. Based on an ultralocal model, research has been conducted on model-free predictive current control (MFPCC) for an induction-motor drive system [14]. The availability of stator current harmonics in a two-level voltage–source inverter means that this approach still has limitations for MFPCC with a finite control set. The performance of FCS-MPC in induction-motor (IM) drives can be improved with the help of a discrete-space vector modulation (DSVM) method, as suggested in [15,16]. Several synthetic virtual voltage vectors are generated in a single sample period using the DSVM method. In [17], a power converter that uses DSVM and FCS-MPC was presented.

This article offers an MFPCC technique that combines an ultralocal model with Discrete-Space Vector Modulation (DSVM) to achieve a more robust and reduced stator current total harmonic distortion (THD). An extended-state observer is implemented to determine the ultralocal model's unknown variables. By comparing THD in stator current, the proposed method outperforms MFPCC-ESO while retaining the same level of dynamic responsiveness. DSVM-MFPCC provides enhanced performance through the generation of several virtual voltage vectors. However, as the number of virtual vectors increases, the calculation burden rises significantly. Here, the sample period divides into two equal time intervals to generate 12 voltage virtual voltage vectors without significantly increasing computation time. The effectiveness of the proposed method is evaluated using a 2.2 kW IM drive whose motor control strategy is FOC. A comprehensive comparison between the proposed method and the conventional MFPCC-ESO has been conducted. Results demonstrate the proposed method's superior performance under various low-speed operating conditions, including regeneration and enhanced motor parameter variation robustness.

2. Induction Motor and Two-Level Voltage–Source Inverter

The two most frequently used methods for controlling electrical motors are field-oriented control (FOC) and direct torque control (DTC) [18–20]. These methods allow stator currents to be closed-loop controlled with outstanding dynamic performance. The first method employs an inner loop to regulate stator current, which provides a voltage reference, and an outer loop to regulate speed and flux. In contrast, the second method employs a lookup table correlating the stator flux position with torque direction and stator flux error. MPC has been implemented in AC drives to regulate the current flowing through the stator (Model Predictive Current Control; MPCC) and to manipulate the torque and flux of the machine directly (Model Predictive Torque Control, MPTC), utilizing these two methods as a foundation [5,6].

The simulation and experiment were performed on the three-phase squirrel-cage induction-motor drives. For a stationary reference frame, the essential electrical and mechanical equations are described as follows [18]:

$$V_s = I_s R_s + \frac{d\Psi_s}{dt}$$

$$0 = I_r R_r + \frac{d\Psi_r}{dt} - j\omega\Psi_r$$

$$\Psi_s = L_s I_s + L_m I_r$$

$$\Psi_r = L_r I_r + L_m I_s$$

$$T_e = \frac{3}{2} p Im\{\overline{\Psi}_s I_s\} \quad (1)$$

where V_s is the stator voltage, I_s and I_r are the stator and rotor current, T_e is the electromagnetic torque, Ψ_s and Ψ_r are the stator and rotor flux, and ω is the speed. The parameters R_s and R_r are the stator and rotor resistances, L_s, L_r, and L_m represent the stator, rotor, and mutual inductances. In the electromagnetic torque equation, $\overline{\Psi}_s$ represents the complex conjugate of Ψ_s, the Im$\{.\}$ operator represents the imaginary component and p is the number of pole pairs.

The dynamic mathematical model for the stator current can be constructed using the previously described IM model [18]:

$$\frac{dI_s}{dt} = -\frac{R_\sigma}{\sigma L_s} I_s + \frac{k_r}{\sigma L_s}\left(\frac{1}{\tau_r} - j\omega\right)\Psi_r + \frac{1}{\sigma L_s} V_s \quad (2)$$

where $\sigma = 1 - k_r k_s$ is the total leakage coefficient, $k_r = \frac{Lm}{Lr}$ and $k_s = \frac{Lm}{Ls}$ are the magnetic coupling factor, $\tau_r = \frac{L_r}{R_r}$ and $R_\sigma = R_s + {k_r}^2 R_r$.

This article employs a traditional three-phase voltage–source inverter (VSI). The inverter is responsible for producing eight real voltage vectors, as illustrated in Figure 1a, and defined by the following equation:

$$V_i = \frac{2}{3} V_{dc}\left(S_1 + aS_2 + a^2 S_3\right) \quad (3)$$

where i = 0, 1, 2, ..., 7 denotes the number of each real voltage vector, S_1, S_2, and S_3 represent the switching phases of the inverter's legs, and a is the constant whose value is $e^{\frac{i2\pi}{3}}$. The magnitudes of two voltage vectors containing zero are considered zero voltage vectors, denoted by V_{s0}(000) and V_{s7}(111). In contrast, the remaining vectors are the real voltage vector—Table 1 lists switching states and voltage vectors.

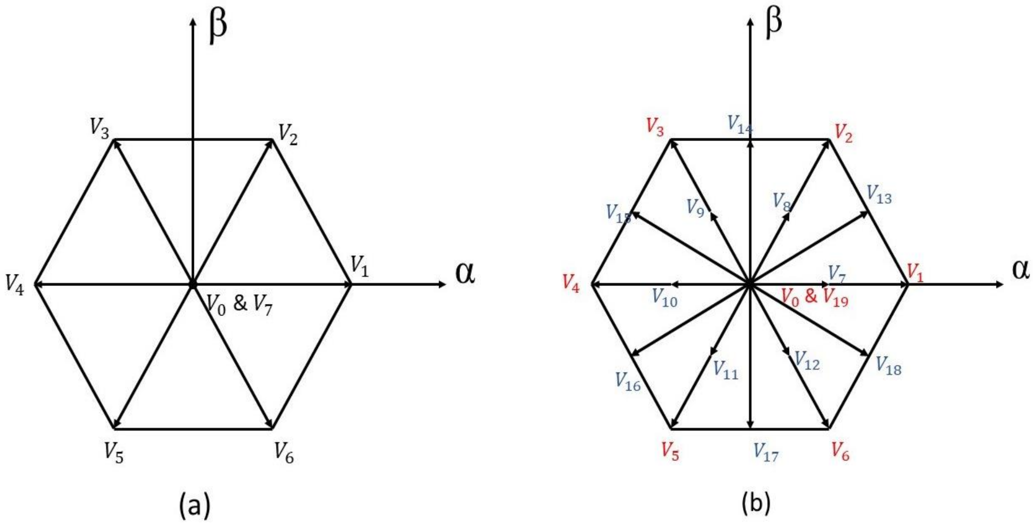

Figure 1. Space Vector Modulation (**a**) Real Voltage Vectors. (**b**) 20 Voltage Vector (real and virtual) for two equal time intervals.

Table 1. Real Voltage Vector with Respective Switching States.

Real Voltage Vector	Switching State [S_1 ,S_2,S_3]
V_{s0}	[0, 0, 0]
V_{s1}	[1, 0, 0]
V_{s2}	[1, 1, 0]
V_{s3}	[0, 1, 0]
V_{s4}	[0, 1, 1]
V_{s5}	[0, 0, 1]
V_{s6}	[1, 0, 1]
V_{s7}	[1, 1, 1]

2.1. Discrete-Space Vector Modulation Method

In the conventional SVM technique, high torque ripple and stator current harmonics are available in a two-level voltage–source inverter due to limited numbers of voltage vectors. To overcome these disadvantages, DSVM was proposed as a viable solution. In DSVM, acquiring a virtual vector in one sampling period for predetermined time intervals is possible. Virtual vectors (V^{vir}) in one sampling period subdivided into an equal N number of intervals for a two-level VSI can be defined as [15,21–23]:

$$V_i^{vir} = \sum_{i=1,2,\ldots N} tV_i^{real} \quad (4)$$

where $V_i^{real} \in \{V_{s0}, V_{s1}, \ldots V_{s7}\}$, and $t = \frac{T_s}{N}$.

The total number of real and virtual voltage vectors can be determined as follows:

$$\text{Total number of voltage vectors} = 3N^2 + 3N + 1 \quad (5)$$

Twenty voltage vectors can be obtained by dividing the sampling period into the same amount of time intervals, as shown in Figure 1b, and their respective values are listed in Table 2. In addition, based on the magnitude of both the real and virtual voltage vectors, Table 3 categorizes the voltage into four groups.

Table 2. Discrete Voltage Vector for N = 2.

Discrete Voltage Vector		
$V_{s0} = 0$	$V_{s8} = \frac{V_{s1}}{2}$	$V_{s14} = \frac{V_{s1}+V_{s2}}{2}$
$V_{s1} = \frac{2}{3}V_{dc}$	$V_{s9} = \frac{V_{s2}}{2}$	$V_{s15} = \frac{V_{s2}+V_{s3}}{2}$
$V_{s2} = V_{s1} + V_{s3}$	$V_{s10} = \frac{V_{s2}}{2}$	$V_{s16} = \frac{V_{s3}+V_{s4}}{2}$
$V_{s3} = V_{s1}\left(-0.5 + 1j\frac{\sqrt{3}}{2}\right)$	$V_{s11} = \frac{V_{s2}}{2}$	$V_{s17} = \frac{V_{s4}+V_{s5}}{2}$
$V_{s4} = V_{s3} + V_{s5}$	$V_{s12} = \frac{V_{s2}}{2}$	$V_{s18} = \frac{V_{s5}+V_{s6}}{2}$
$V_{s5} = \left(-0.5 - 1j\frac{\sqrt{3}}{2}\right)$	$V_{s13} = \frac{V_{s2}}{2}$	$V_{s19} = \frac{V_{s6}+V_{s1}}{2}$
$V_{s6} = V_{s1} + V_{s5}$		$V_{s7} = 0$

Table 3. Vector Control Set.

Index	Discrete Voltage Vector
Real	$V_{s1}, V_{s2}, V_{s3}, V_{s4}, V_{s5}, V_{s6}$
Short	$V_{s8}, V_{s9}, V_{s10}, V_{s11}, V_{s12}, V_{s13}$
Large	$V_{s14}, V_{s15}, V_{s16}, V_{s17}, V_{s18}, V_{s19}$
Zero	V_{s0}, V_{s7}

2.2. Model-Free Predictive Current Control of Induction Motor

Knowing the system model is crucial for the MPC algorithm's performance. However, it is common for the system's parameters to shift over time. Therefore, such a model should include temporal variation. The problem is that obtaining such a model would impose undesirable computing overhead on the practical implementation of the control system. Additionally, there is the problem of developing a foolproof initial parameter identification technique for an unknown plant. In extreme circumstances, performance loss and control instability might result from a mismatch between the model and the controlled parameters.

An alternative strategy is to use Model-Free Predictive control. The methodologies are divided into three categories based on their dependency on models. First, strictly model-free prediction does not rely on models. Instead, a lookup table makes predictions based on the system's past input and output data. Second, it employs an ultralocal model, which utilizes a model alongside one or more undefined variables that must be continuously estimated based on the system's input and output data. Thirdly, Prediction Correction methods employ an idealized plant model. Nevertheless, correction factors are evaluated to compensate for the predictions using the system's input, output, and previous prediction data.

2.2.1. Ultralocal Model-Based MFPCC

For a single input U and single output Y, an ultralocal model can replace the unknown complex mathematical model. The complex vector-based ultralocal dynamic model for the stator current of an induction motor in a stationary frame as [13,24]:

$$\frac{dI_s}{dt} = \alpha V_s + F \tag{6}$$

From Equation (2), $F = -\frac{R_\sigma}{\sigma L_s} I_s + \frac{k_r}{\sigma L_s}\left(\frac{1}{\tau_r} - j\omega\right)\psi_r$ is considered to be an unknown component, while $\alpha = \frac{1}{\sigma L_s}$ represent the scaling factor of the input voltage vector V_s. Taking α as a constant, $I_s(x+1)$ can be determined by estimating F using an ESO-based observer.

2.2.2. MFPCC Parameter Design

Based on the above equation, a linear extended-state observer can be designed by employing an unknown part F and stator current I_s as a state variable along with feedback of error in a stator current e_{rr} as [14]:

$$e_{rr}(x) = I_s^{ref}(x) - I_s(x)$$

$$\hat{I}_s(x+1) = I_s(x) + T_s\left(\hat{F}(x) + \alpha V_s(x)\right) - \beta_{01} e_{rr}(x)$$

$$\hat{F}(x+1) = \hat{F}(x) - \beta_{02} e_{rr}(x) \tag{7}$$

where $\hat{I}_s(x+1)$ represents the predicted stator current $I_s(x)$, $\hat{F}(x)$ is the approximated value of F, and for $z \in (0,1)$ $\beta_{01} = 2(1-z)$ and $\beta_{02} = \frac{(1-z)^2}{T_s}$, represent the observer's error feedback gain, while z is set to 0.15.

3. Proposed DSVM-Based MFPCC

The control block diagram for the proposed method is shown in Figure 2, while Figure 3 is a flowchart illustrating the proposed method. From Equation (6) and the unit step delay in the reference stator current, the reference voltage can be determined as:

$$V_s(x+1) = \frac{I_s^{ref}(x+2) - \hat{I_s}(x+1)}{\alpha T_s} - \frac{\hat{F}(x+1)}{\alpha} \tag{8}$$

where $V_s(x+1)$ is the applied voltage vector at an instant $(x + 1)$. To compute the difference between I_s^{ref} and I_s, the following cost function is constructed:

$$g = \left|\frac{I_s^{ref}(x+2) - I_s(x+1)}{\alpha} - T_s\left(V_s(x+1) - \frac{\hat{F}(x+1)}{\alpha}\right)\right|^2 \tag{9}$$

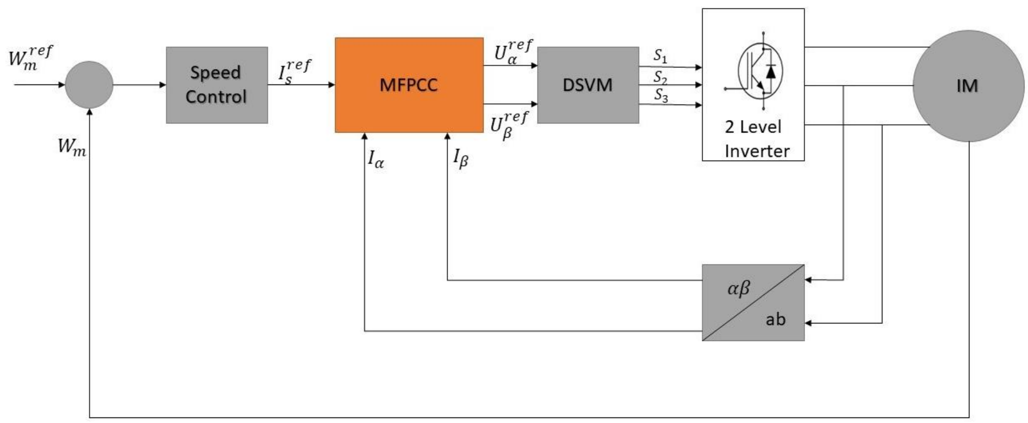

Figure 2. Control diagram of the proposed DSVM-MFPCC induction-motor drive system.

The voltage vector $V_s(x+1)$ must be applied to acquire the minimum value of the cost function $g \cong 0$. Since DSVM is a type of finite-control set predictive control, the voltage vector $V_s(x+1)$ is not always a member of the finite-control set vectors. Therefore, the voltage vector closest to the $V_s(x+1)$ should be selected as optimal V_{opt} to minimize the cost function. To minimize the cost function, select an optimal V_{opt} that is close to the voltage vector $V_s(x+1)$.

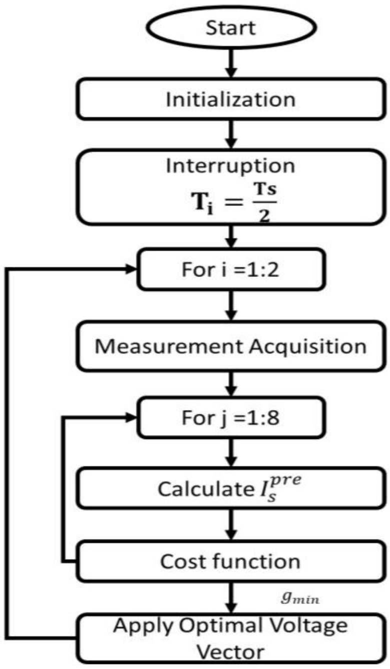

Figure 3. Flowchart of the proposed DSVM-MFPCC.

4. Results

Simulation and experimental testing using squeal-cage induction-motor drivers on a two-level voltage–source inverter validate the effectiveness of the proposed method. Table 4 contains a description of the control system parameters that were implemented in the simulation and experimental configuration. The sampling frequency is 10 kHz, and the values of β_{01} and β_{02} are 1.7 and 7225, respectively. Here, four parameters stator current in the DQ axis I_d and I_q, speed W_m and stator current I_a (phase A current) are observed. The I_d is directly proportional to the stator flux and I_q is directly proportional to the torque. Keeping stator flux constant, the torque generated only depends on I_q.

Table 4. Induction-motor parameters.

Induction-Motor Parameters	Symbols	Value
DC Voltage	V_{dc}	700 V
Rated Power	P_N	2.2 kW
Rated Voltage	V_N	415 V
Rated Current	I_N	4.4 A
Rated Frequency	f_N	50 Hz
Rated Torque	T_N	14 Nm
Pole Pairs	p	2
Stator Resistance	R_s	4.125 Ohm
Stator Inductance	L_s	300.37 mH
Rotor Resistance	R_r	2.486 Ohm
Rotor Inductance	L_r	300.37 mH
Mutual Inductance	L_m	284.80 mH

4.1. Simulation Results

In MATLAB/Simulink, a simulation comparison of the conventional ultralocal model base MFPCC and the proposed DSVM-MFPCC is conducted. Figure 4 illustrates the simulation results of the conventional ultralocal model base MFPCC and the proposed DSVM-MFPCC with precise IM parameters. The test condition can observe the performance of the proposed method, in that the speed reference steps up from 0 to 1000 rpm at t = 0 s, and a sudden load torque of 10 Nm is applied at t = 6 s. It can be observed that when load torque is applied, I_q increases and restores the induction motor's speed. These conditions help to observe the transient and dynamic response of the control system.

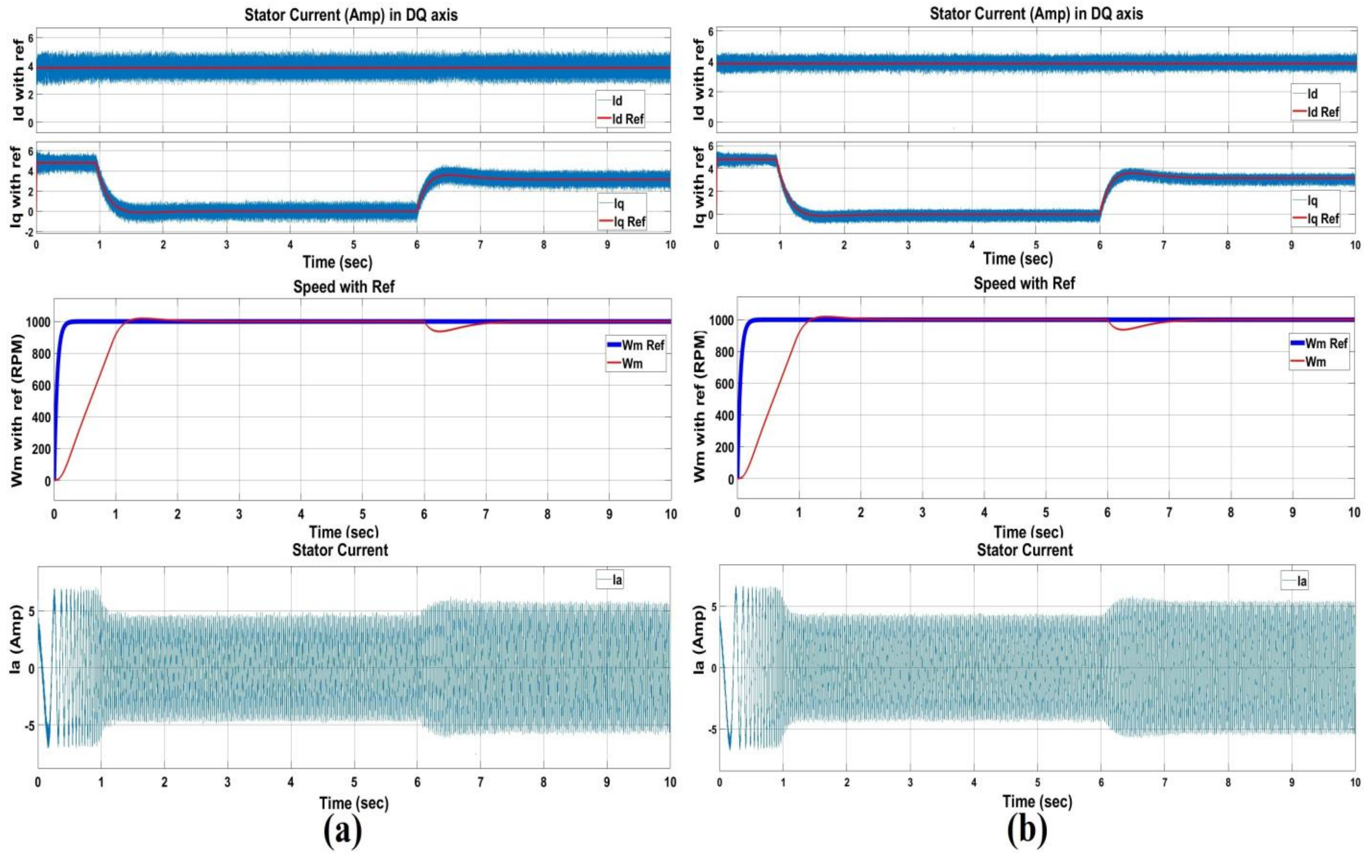

Figure 4. Simulated dynamic response at 1000 rpm for (**a**) MFPCC and (**b**) DSVM–MFPCC.

Similarly, in Figure 5, the test condition is that the reference speed increases from 0 to 1000 rpm at t = 0 s, followed by applying an abrupt load torque of 10 Nm at t = 6 s, and observes the similar speed recovery which evaluate the performance of the proposed method concerning the mismatch parameter. The motor parameters change to $L_s{}' = 0.8\ L_s$ and $R_s{}' = 0.5\ R_s$. The 1st channel presents the reference and stator current in the DQ axis, the 2nd channel presents the reference and actual speed, and the 3rd channel displays the phase A stator current. Observations indicate that conventional MFPCC has more significant ripples in stator current than the proposed DSVM-MFPCC.

Figures 4 and 5 depict the responses for exact and mismatched parameters for starting at the rated speed and reversing at the rated speed, respectively. The proposed DSVM-MFPCC performs similarly to the conventional MFPCC. With a sampling frequency of 10 kHz and at the speed of 1000 rpm, it is observed that conventional MFPCC has a THD of 14.34%. By contrast, the proposed method reduces the THD to 7.13%. Also, for mismatch parameters, the THD is 14.97% for conventional MFPCC and 7.61% for the proposed method, a reduction of approximately 50% compared to conventional MFPCC. Similar to conventional MFPCC, the proposed method demonstrates outstanding dynamic performance.

In Figure 6, the test condition is that the speed reference steps from 100 rpm to 500 rpm at t = 4 s to analyze the performance of the proposed method under low-speed applications. In addition, the simulation results show that the proposed method is effective, as stator current THD is 17.93% for conventional MFPCC and 9.14% for proposed DSVM-MFPCC. Therefore, the proposed method THD is improved compared to the MFPCC method under different operating conditions. Figure 7a displays the current THD for the various simulation conditions, from which it can be concluded that the THD for the low-speed operation of an induction motor is more significant than for high-speed operation.

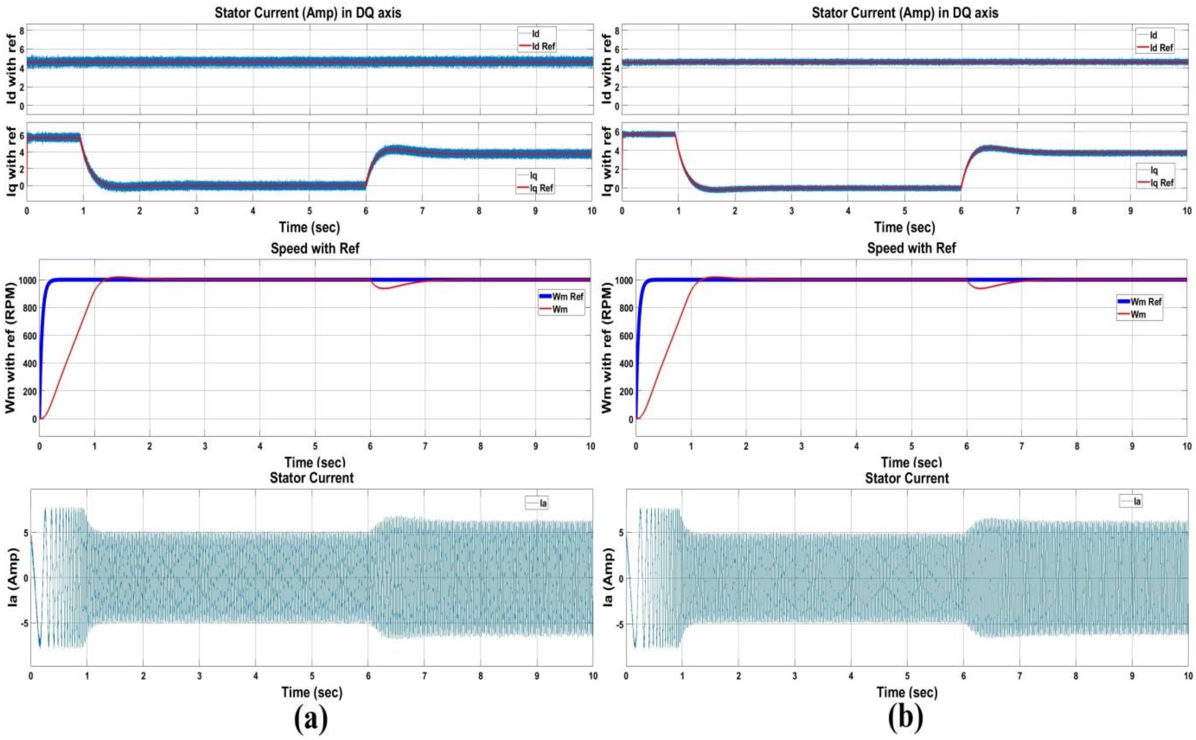

Figure 5. Simulated dynamic response at 1000 rpm for under mismatch parameter: (**a**) MFPCC; and (**b**) DSVM–MFPCC.

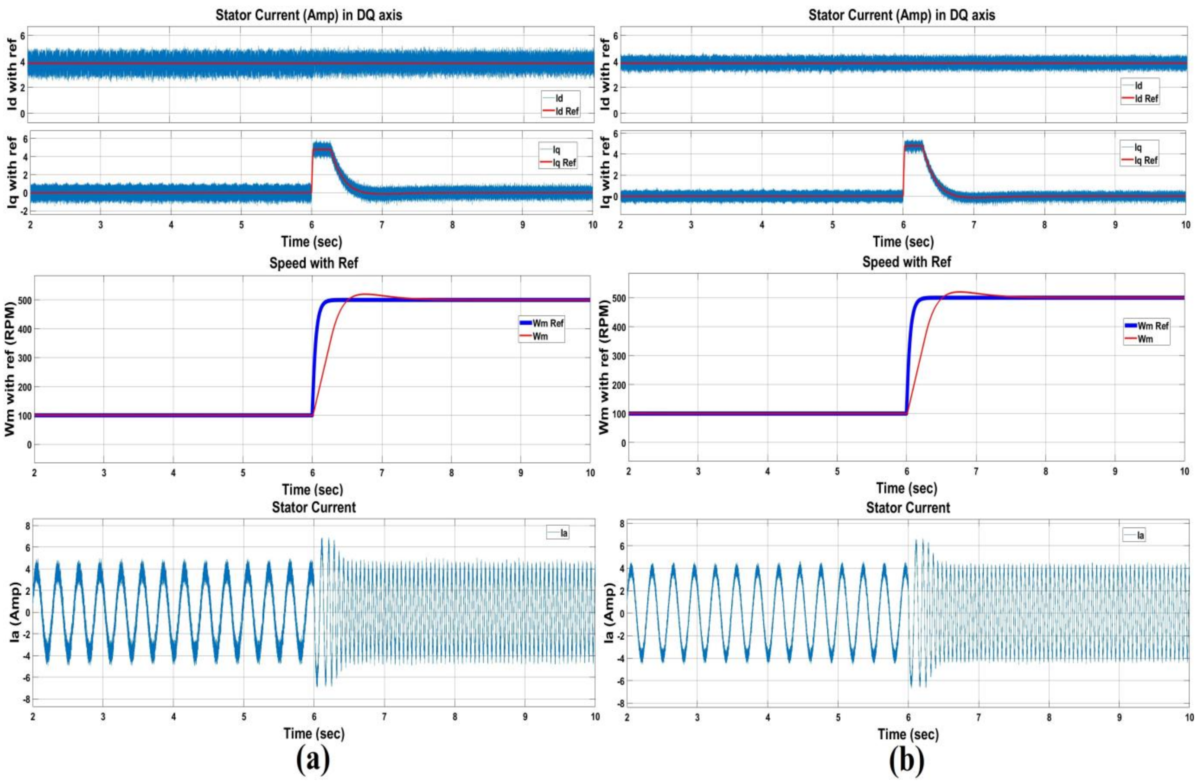

Figure 6. Simulated dynamic response at low speed: (**a**) MFPCC; and (**b**) DSVM–MFPCC.

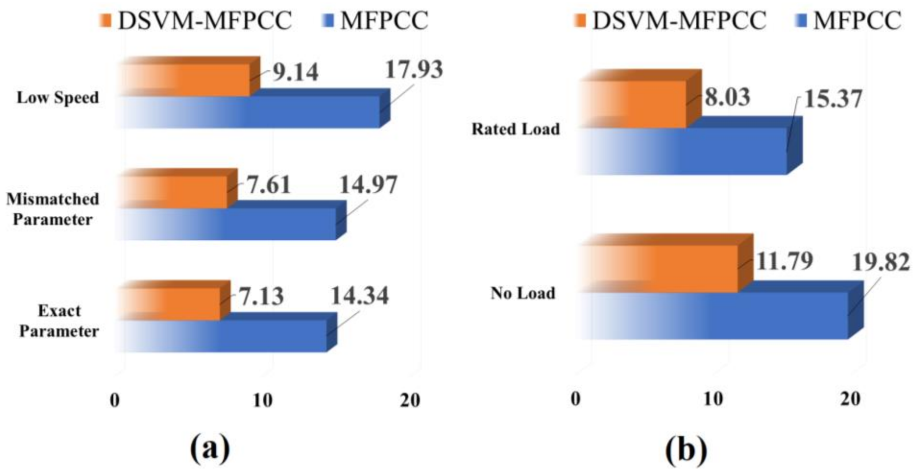

Figure 7. Current THD (**a**) for different simulation conditions, (**b**) for no-load and rated-load conditions.

An induction-motor drive's optimal performance and efficiency depend significantly on its low-speed performance. Various factors, including motor parameters, load characteristics, and control strategy, influence the low-speed performance of the motor drive. Therefore, analyzing and optimizing its low-speed performance is essential to ensure that the motor drive operates reliably and efficiently over a wide range of speeds and loads. In Figure 6b, the simulated result shows the performance of the induction motor at low speed. The proposed method performs better with less current ripple than the conventional MFPCC.

4.2. Experimental Results

The proposed DSVM-MFPCC and MFPCC are experimentally tested on a 2-Level 3 ph voltage–source inverter module fed 2.2 kW/415 V/50 Hz IM, as shown in Figure 8. The control of rotor speed and phase A stator current are displayed via NI-based LabView 2023 Q1. All waveforms are displayed by a waveform graph available in the control palette in LabView.

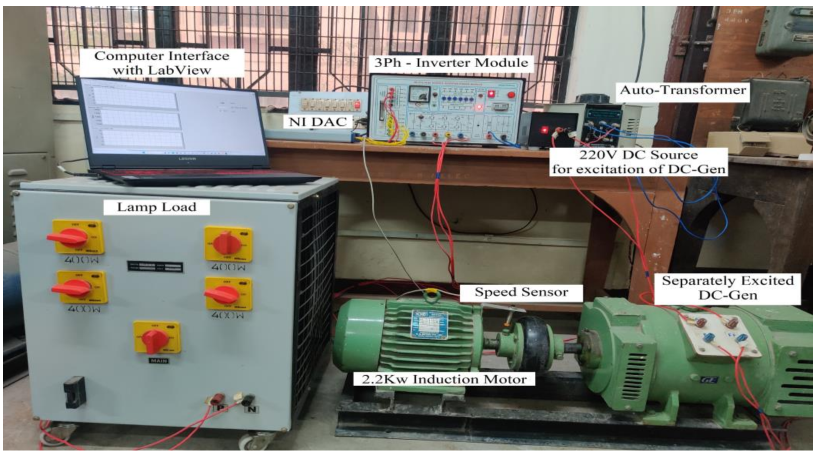

Figure 8. Experimental Setup.

Figure 9 illustrates the starting response and reference speed taken from zero to the rated speed, then a speed reversal at the rated speed for the two methods. A sampling frequency is taken at 10 kHz throughout the experiment. Similar to conventional MPCC, the proposed method displays outstanding dynamic performance. For conventional MFPCC-ESO, the current ripple is evident. However, for DSVM-MFPCC, the current ripple is diminished. The THD calculated for the MFPCC is 19.82%, and for the DSVM-MFPCC, it is 11.79% for the no-load condition. Therefore, the experimental results correspond to Figure 4's simulation results.

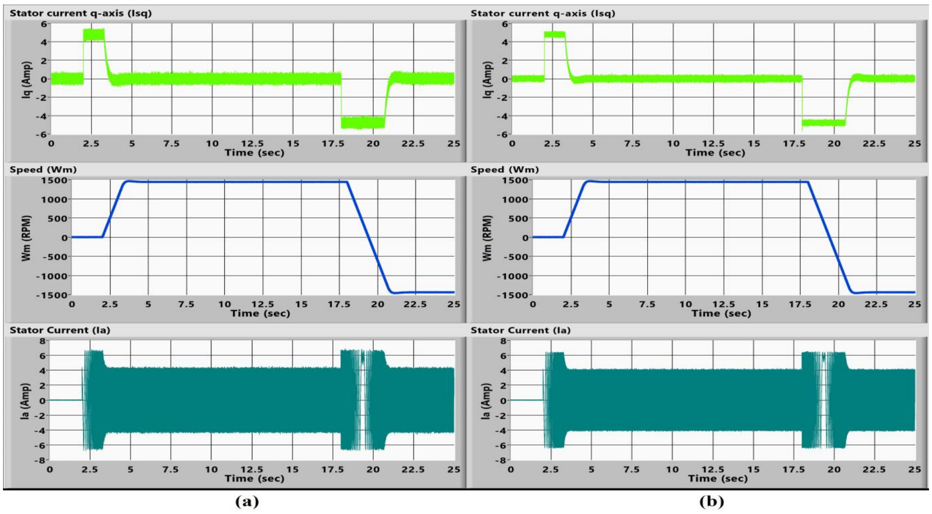

Figure 9. Starting responses to rated speed and reversal at rated speed: (**a**) MFPCC; and (**b**) DSVM–MFPCC.

Figure 10 illustrates the dynamic response to a step-load torque change from 0% to 50%, then 100% of the rated load with the help of the load lamp, as shown in Figure 8. The THD calculated for the rated-load condition is 15.37% for MFPCC and 8.03% for DSVM-MFPCC. Figure 7b displays the current THD for the no-load conditions and rated-load condition, from which it can be concluded that the THD for the no-load condition of an induction motor has a higher value than for the rated-load condition. Figure 10 demonstrates the experimental results with the same speed recovery characteristics as Figures 4 and 5. The dynamic responses of the two methods are alike. To compensate for the sudden load, the q-axis current rises rapidly, and the motor speed recovers to its reference value. Studies validate the suggested method's efficiency in generating a rapid dynamic response.

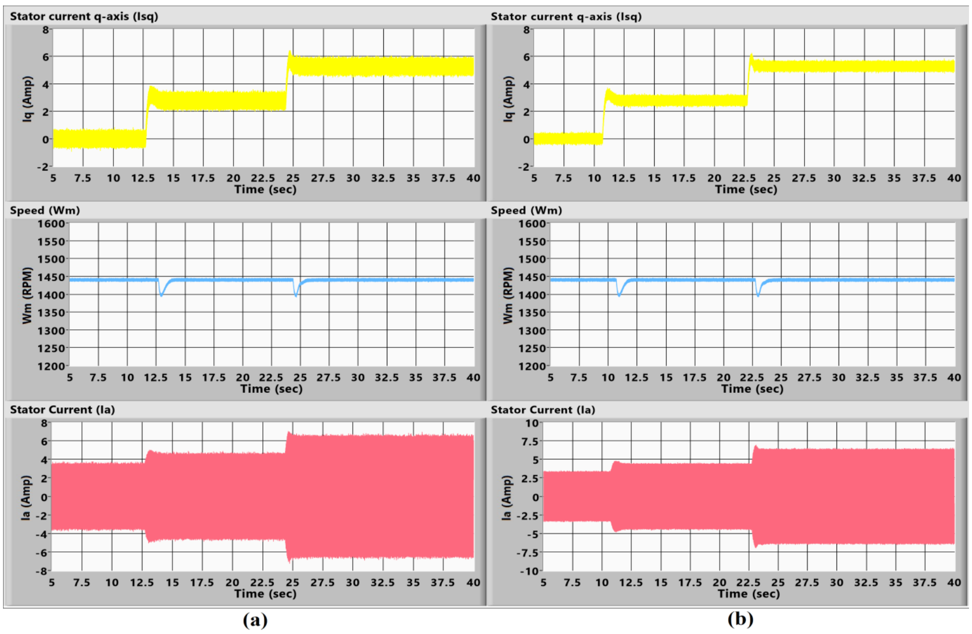

Figure 10. Dynamic responses to stepped load torque change from 0 to 50% to 100%: (**a**) MFPCC; and (**b**) DSVM–MFPCC.

5. Conclusions

This paper presents a model-free predictive current control based on discrete-space vector modulation for induction-motor drives that do not depend on motor parameters and exhibit resilient parameter robustness. It has a straightforward concept and is simple to implement. The simulation and experimental results demonstrated that the effectiveness of the proposed DSVM-MFPCC and conventional MFPCC are comparable. In contrast, DSVM-MFPCC performed better than MPFCC regarding stator current ripple under both conditions, i.e., exact parameters and mismatch parameters, resulting in about a 50% reduction. Also, THD may vary under different simulation and load conditions, but DSVM-MFPCC performed better than MPFCC in all conditions. The simulation and experimental studies illustrated that the suggested method obtains excellent reliability and effectiveness to the induction-motor drive. Additionally, a motor's low-speed efficacy is enhanced by a reduction in current ripple, demonstrating a more accurate estimation of the unknown variable F of the ultralocal model of IM in conjunction with a significant reduction in steady-state fluctuations over a broad range.

Author Contributions: Conceptualization, M.A.H. and A.S.H.; Data curation, M.A.H., A.S.H. and V.B.; Formal analysis, V.P. and P.C.; Investigation, B.T.H. and P.C.; Methodology, M.A.H., A.S.H. and V.B.; Resources, V.B., B.T.H. and V.P.; Software, M.A.H., V.B. and B.T.H.; Supervision, A.S.H., V.B., B.T.H., V.P. and P.C.; Validation, A.S.H., V.P. and P.C.; Visualization, M.A.H. and V.B.; Writing—original draft, M.A.H., A.S.H., V.P. and P.C.; Writing—review and editing, M.A.H., A.S.H., V.B. and B.T.H. All authors have read and agreed to the published version of the manuscript.

Funding: This research received no external funding.

Data Availability Statement: Data sharing is not applicable.

Conflicts of Interest: The authors declare no conflict of interest.

References

1. Cortes, P.; Kazmierkowski, M.P.; Kennel, R.M.; Quevedo, D.E.; Rodriguez, J. Predictive Control in Power Electronics and Drives. *IEEE Trans. Ind. Electron.* **2008**, *55*, 4312–4324. [CrossRef]
2. Kouro, S.; Cortes, P.; Vargas, R.; Ammann, U.; Rodriguez, J. Model Predictive Control—A Simple and Powerful Method to Control Power Converters. *IEEE Trans. Ind. Electron.* **2008**, *56*, 1826–1838. [CrossRef]
3. Rodriguez, J.; Kazmierkowski, M.P.; Espinoza, J.R.; Zanchetta, P.; Abu-Rub, H.; Young, H.A.; Rojas, C.A. State of the Art of Finite Control Set Model Predictive Control in Power Electronics. *IEEE Trans. Ind. Inform.* **2012**, *9*, 1003–1016. [CrossRef]
4. Mousavi, M.S.; Davari, S.A.; Nekoukar, V.; Garcia, C.; Rodriguez, J. Finite-Set Model Predictive Current Control of Induction Motors by Direct Use of Total Disturbance. *IEEE Access* **2021**, *9*, 107779–107790. [CrossRef]
5. Rodriguez, J.; Garcia, C.; Mora, A.; Flores-Bahamonde, F.; Acuna, P.; Novak, M.; Zhang, Y.; Tarisciotti, L.; Davari, S.A.; Zhang, Z.; et al. Latest Advances of Model Predictive Control in Electrical Drives—Part I: Basic Concepts and Advanced Strategies. *IEEE Trans. Power Electron.* **2021**, *37*, 3927–3942. [CrossRef]
6. Zhang, Y.; Yang, H.; Xia, B. Model-Predictive Control of Induction Motor Drives: Torque Control Versus Flux Control. *IEEE Trans. Ind. Appl.* **2016**, *52*, 4050–4060. [CrossRef]
7. Prince; Hati, A.S.; Chakrabarti, P.; Abawajy, J.H.; Keong, N.W. Development of energy efficient drive for ventilation system using recurrent neural network. *Neural Comput. Appl.* **2021**, *33*, 8659–8668. [CrossRef]
8. Prince; Hati, A.S.; Kumar, P. An adaptive neural fuzzy interface structure optimisation for prediction of energy consumption and airflow of a ventilation system. *Appl. Energy* **2023**, *337*, 120879. [CrossRef]
9. Prince; Hati, A.S. A comprehensive review of energy-efficiency of ventilation system using Artificial Intelligence. *Renew. Sustain. Energy Rev.* **2021**, *146*, 111153. [CrossRef]
10. Kumar, P.; Hati, A.S. Sensor-less Speed Control of Ventilation System Using Extended Kalman Filter For High Performance. In Proceedings of the 2021 IEEE 8th Uttar Pradesh Section International Conference on Electrical, Electronics and Computer Engineering (UPCON), Dehradun, India, 11–13 November 2021; pp. 1–6. [CrossRef]
11. Boileau, T.; Leboeuf, N.; Nahid-Mobarakeh, B.; Meibody-Tabar, F. Online Identification of PMSM Parameters: Parameter Identifiability and Estimator Comparative Study. *IEEE Trans. Ind. Appl.* **2011**, *47*, 1944–1957. [CrossRef]
12. Dang, D.Q.; Rafaq, M.S.; Choi, H.H.; Jung, J.-W. Online Parameter Estimation Technique for Adaptive Control Applications of Interior PM Synchronous Motor Drives. *IEEE Trans. Ind. Electron.* **2015**, *63*, 1438–1449. [CrossRef]
13. Fliess, M.; Join, C. Model-free control and intelligent PID controllers: Towards a possible trivialization of nonlinear control? *IFAC Proc. Vol.* **2009**, *42*, 1531–1550. [CrossRef]

14. Zhang, Y.; Wang, X.; Zhang, B.; Yang, H. A Robust Model-Free Predictive Current Control of Induction Motor Drives. In Proceedings of the 2019 22nd International Conference on Electrical Machines and Systems (ICEMS), Harbin, China, 11–14 August 2019; pp. 1–5. [CrossRef]
15. Casadei, D.; Serra, G.; Tani, K. Implementation of a direct control algorithm for induction motors based on discrete space vector modulation. *IEEE Trans. Power Electron.* **2000**, *15*, 769–777. [CrossRef]
16. Wei, X.; Chen, D.; Zhao, C. Minimization of torque ripple of direct-torque controlled induction machines by improved discrete space vector modulation. *Electr. Power Syst. Res.* **2004**, *72*, 103–112. [CrossRef]
17. Vazquez, S.; Leon, J.I.; Franquelo, L.G.; Carrasco, J.M.; Martinez, O.; Rodríguez, J.; Cortes, P.; Kouro, S. Model Predictive Control with constant switching frequency using a Discrete Space Vector Modulation with virtual state vectors. In Proceedings of the 2009 IEEE International Conference on Industrial Technology, Gippsland, Australia, 10–13 February 2009; pp. 1–6.
18. Holtz, J. The representation of AC machine dynamics by complex signal flow graphs. *IEEE Trans. Ind. Electron.* **1995**, *42*, 263–271. [CrossRef]
19. Le-Huy, H. Comparison of field-oriented control and direct torque control for induction motor drives. In Proceedings of the Conference Record of the 1999 IEEE Industry Applications Conference. Thirty-Forth IAS Annual Meeting (Cat. No.99CH36370), Phoenix, AZ, USA, 3–7 October 1999; Volume 2, pp. 1245–1252. [CrossRef]
20. Alberti, L.; Bianchi, N.; Bolognani, S. Field oriented control of induction motor: A direct analysis using finite element. In Proceedings of the 2008 34th Annual Conference of IEEE Industrial Electronics, Orlando, FL, USA, 10–13 November 2008; pp. 1206–1209. [CrossRef]
21. Osman, I.; Xiao, D.; Alam, K.S.; Shakib, S.M.S.I.; Akter, P.; Rahman, M.F. Discrete Space Vector Modulation-Based Model Predictive Torque Control With No Suboptimization. *IEEE Trans. Ind. Electron.* **2019**, *67*, 8164–8174. [CrossRef]
22. Gonzalez-Prieto, I.; Duran, M.J.; Aciego, J.J.; Martin, C.; Barrero, F. Model Predictive Control of Six-Phase Induction Motor Drives Using Virtual Voltage Vectors. *IEEE Trans. Ind. Electron.* **2017**, *65*, 27–37. [CrossRef]
23. Wang, T.; Zhu, J. Finite-control-set model predictive direct torque control with extended set of voltage space vectors. In Proceedings of the 2017 20th International Conference on Electrical Machines and Systems (ICEMS), Sydney, Australia, 11–14 August 2017; IEEE: Piscataway, NJ, USA; pp. 1–6.
24. Fliess, M.; Join, C. Model-free control. *Int. J. Control* **2013**, *86*, 2228–2252. [CrossRef]